Apparent Roughness in Wave–Current Flow: Implication for Coastal Studies

Alexander Perlin[1] and Eliezer Kit[2]

Abstract: High turbulence intensities generated by waves in the wave bottom boundary layer affect the mean current velocity and should be taken into account for calculation of currents in the presence of waves. This influence of the wave-induced turbulence on the mean current can be schematized by introducing an ''apparent'' bed roughness, which is larger than the physical bottom roughness. Apparent bed roughness is defined here as roughness that provides the same depth-mean velocity for current alone configuration as for the wave–current flow. A one-dimensional vertical ''$k-l$'' turbulence closure model that allows detailed time dependent flow modeling has been applied for apparent roughness computations. The domain of variable parameters is chosen according to the Israeli near-shore conditions. An approximate expression for apparent bed roughness calculations as a function of wave and current parameters based on this turbulence closure model is derived. Simulation of flow patterns on the Tel Aviv coast using the three-dimensional Costal and Marine Engineering Research Institute flow model and implementing apparent roughness maps, calculated by the approximate expression, has been performed.

DOI: 10.1061/(ASCE)0733-9429(2002)128:8(729)

CE Database keywords: Roughness; Waves; Turbulence; Boundary layers.

Introduction

In the coastal environment, waves and currents are more often than not present at the same time. Thus, a motion characterized as the combined motion of waves and currents may be considered the most commonly encountered flow condition in near-coastal waters. The effect of the presence of waves on the characteristics of a current is intimately related to the processes taking place within the wave boundary layer. Although the thickness of the wave turbulent boundary layer is quite small when compared to the water depth, it still plays a very important role in determining the rate of water fluxes, sediment transport, and other important engineering characteristics. As a consequence of near-bottom wave–current interaction, the prediction of the near-bottom wave–current velocity profile is sensitive to the presence of waves. This influence of the wave induced turbulence on the mean current can be schematized by introducing an ''apparent'' bed roughness, which is larger than the physical bottom roughness (Madsen 1991).

Laboratory experiments do not always confirm this trend of shear stress magnification by superimposing of oscillatory motion on a steady current. For example, the work by Lodahl et al. (1998) indicates that in a smooth pipe mean wall shear stress may increase, may retain its steady current value, or even decrease, depending on the flow regime. Arnskov et al. (1993) observed that turbulence was suppressed by waves propagating either perpendicularly or obliquely to the flow, although bed shear stress increased. It should be stressed, however, that the Reynolds number of the wave boundary layer in the Arnskov et al. (1993) experiment was relatively small, such that the flow generated by waves was laminar. Laboratory measurements in the boundary layers over a rough bottom, reported by Simons et al. (1992), show an increase in mean shear stress when waves propagate at a right angle to the current. However, Simons et al. (1992) find that the shear stress is sometimes considerably lower than predicted by theory, with the greatest discrepancies occurring in waves with the shortest wave periods and the lowest Reynolds numbers.

Several attempts have been made to evaluate the apparent bed roughness. Based on the data, which was available at the time, and utilizing a zero-equation turbulence model, Coffey and Nielsen (1986) suggested that it may be possible to express the apparent roughness increase as a function of a single parameter, namely the ratio of maximum to mean friction velocity. Sleath (1990) however found that this formula seemed inadequate for data with smaller relative roughness. Subsequently Sleath (1991) developed another model that established the apparent roughness increase as a function of two parameters: the ratio of near-bed wave orbital velocity to mean current friction velocity and the ratio of the amplitude of wave orbital motion to bed roughness. Nielsen's (1992) expression based on the zero-equation model shows that the increase in apparent roughness is proportional to the ratio of near-bed wave orbital velocity to the mean current friction velocity.

Fredsøe and Deigaard (1992) determined the apparent roughness by matching the inner and the outer mean current profile in the mean thickness of the boundary layer for the Fredsøe (1984) turbulence model. The solution of the Fredsøe (1984) model provided the dependence of the apparent bed roughness on the following parameters: ratio of near-bed wave orbital velocity to mean current friction velocity, ratio of amplitude of wave orbital

[1]PhD student, Dept. of Fluid Mechanics and Heat Transfer, Tel Aviv Univ., Ramat-Aviv 69978, Israel.

[2]Professor, Dept. of Fluid Mechanics and Heat Transfer, Tel Aviv Univ., Ramat-Aviv 69978, Israel.

Note. Discussion open until January 1, 2003. Separate discussions must be submitted for individual papers. To extend the closing date by one month, a written request must be filed with the ASCE Managing Editor. The manuscript for this paper was submitted for review and possible publication on October 3, 2000; approved on February 8, 2002. This paper is part of the ***Journal of Hydraulic Engineering***, Vol. 128, No. 8, August 1, 2002. ©ASCE, ISSN 0733-9429/2002/8-729–741/$8.00+$.50 per page.

motion to bed roughness, and angle between waves and current. However, in order to use their model for computation of the apparent bed roughness, the entire solution has to be obtained. A weak point of their model is an assumption of a logarithmic velocity profile both in the outer part of the flow and in the wave boundary layer. While this assumption works well for the outer profile, the inner profile is not exactly logarithmic. Moreover, an intermediate layer exists between the inner and outer profiles. While inner and intermediate layers are much thinner, turbulence intensities are generated mostly in these layers. Therefore for the apparent roughness computations the proper modeling of these layers is important.

A variety of models for the vertical structure of the wave–current bottom boundary layer have been proposed in recent years. Most of the later theories made use of an eddy viscosity assumption in which the viscosity was held constant in time, even for time-varying flow, and varied in the vertical direction according to some prescribed functional form (Lundgren 1973; Smith 1977; Grant and Madsen 1979; Tanaka and Shuto 1981; Tanaka et al. 1983; Myrhaug 1984; Christoffersen and Jonsson 1985; Coffey and Nielsen 1985; and Madsen 1991).

In a two-equation model, the length scale l is allowed to vary in time and space instead of being given by a prescribed function. This additional equation is usually a transport equation for the dissipation ϵ, which is structured similarly to the equation for turbulent kinetic energy k and both are derived from the Navier–Stokes equations. This results in a so-called "$k-\epsilon$" model. Models of this type have been used by Celik and Rodi (1984) to study the free-surface effect, and by Justesen (1988) to study oscillatory boundary layer flow. An alternative method is to derive a transport equation for the length scale and to include it in a turbulence closure scheme (Davies 1986, 1990, 1991; Davies et al. 1988; Li and Davies 1996). In general, models of the combined wave and current bottom boundary layer have assumed the flow to be horizontally uniform, and have aimed to predict "at a point" the vertical distribution of properties such as the fluid velocity, shear stress, and turbulence intensity.

The numerical model chosen in the current work is similar to that presented by Davies et al. (1988), and is based on a "$k-l$" turbulence closure model for the wave–current boundary layer. The equation for l is obtained from, modified by Bobyleva et al. (1965), the von Kármán's (1930) idea of calculating the length scale from local derivatives of the velocity. This model allows greater sophistication in the determination of a time-varying eddy viscosity than the simple models. The model does not put any constraints on: (1) the shape of the current profile, (2) mutual orientation of waves and current, and (3) combination of small waves with strong currents or the opposite. The overall objective of the present research is to develop a method, based on the sophisticated numerical model, aimed at calculating the apparent bed roughness. The apparent bed roughness then can be used for calculations of current in the presence of waves in coastal regions with complicated bathometry by applying a three-dimensional (3D) flow model. An example of such a model is the Coastal and Marine Engineering Research Institute (CAMERI) flow model (Sladkevich et al. 2000), which is very efficient in the simulation of transport phenomena in a shallow aquatic environment.

Successful use of this model requires that the apparent bed roughness be evaluated for the conditions that are typical for sediment transport calculations, that is, the wave-breaking zone on sandy beaches, and the result should be easily incorporated into a 3D model. The domain for wave and current properties' variation is chosen according to Israeli near-shore conditions. An approximate expression for the apparent bed roughness calculations within the selected domain is derived based on numerical simulations of the wave–current boundary layer.

The wave roughness map of the region, calculated by this approximate expression, is used as an input parameter to the 3D model. Feedback from the 3D model is realized through an additional driving force that can be added to the initial driving forces. The additional driving force of pressure gradient type is an effect of horizontal nonuniformity of the flow that is modeled by the 3D model. Wave roughness is recalculated with this additional driving force and then used again in the 3D model. The flow pattern calculated by the 3D model with the implementation of wave roughness is compared with the flow pattern obtained without taking into account the influence of the wave–current bottom boundary layer on the mean current. The essential difference between these patterns is demonstrated and analyzed.

Turbulence Closure Model for Combined Wave and Current Flow

The turbulence numerical model used in the present work differs from the Davies et al. (1988) model by introducing the possibility of applying the shear stress on the free surface as a boundary condition for momentum equations instead of the zero velocity gradient. The present model also enables use of various types of boundary conditions for the equation for turbulent energy. The motion in the wave–current boundary layer is obtained from the numerical model in two stages. First, the model is used to provide a one-dimensional, horizontally uniform starting current between the free surface and the flat hydrodynamically rough bed. Second, a horizontally uniform wave motion of prescribed frequency is added to the current at the angle of attack ϕ. The model is then allowed to converge to the combined wave and current steady state forced by the same mean pressure gradient.

If the assumption of horizontal uniformity in the flow is valid, the unsteady boundary layer approximation to the Reynolds-averaged horizontal momentum equations has the form

$$\frac{\partial U}{\partial t}=-\frac{1}{\rho}\frac{\partial p}{\partial x}+\frac{\partial}{\partial z}(\tau_{zx}/\rho) \tag{1}$$

$$\frac{\partial V}{\partial t}=-\frac{1}{\rho}\frac{\partial p}{\partial y}+\frac{\partial}{\partial z}(\tau_{zy}/\rho) \tag{2}$$

where x = horizontal coordinate; U and V = horizontal component of velocity in the x and y directions; τ_{zx} = Reynolds stress in the x direction; and τ_{zy} = Reynolds stress in the y direction.

The no-slip condition for a rough bed can be written as

$$U=0,\quad V=0 \quad \text{at } z=z_0 \tag{3}$$

where z_0 = bed level, which according to Nikuradse (1932) can be taken equal to $k_d/30$, where k_d = bed roughness. At the free surface the following conditions are applied:

$$\tau_{zx}=0,\quad \tau_{zy}=\tau_s \quad \text{at } z=h \tag{4}$$

where τ_s = surface shear stress due to the wind. For convenience, the wind direction is chosen to coincide with the y coordinate.

For shallow water the amplitude of the wave orbital velocity remains almost constant outside the boundary layer and the free stream velocity can be written

$$V_0=u_b\cos\sigma t \tag{5}$$

Therefore, for wave motion of potential velocity amplitude u_b superimposed on a current at the angle ϕ, the pressure gradients are equal to

$$-\frac{1}{\rho}\frac{\partial p}{\partial x}=\frac{\mathrm{d}U_x}{\mathrm{d}t}+P_x \tag{6}$$

where $U_x=u_b \sin\phi\cos\sigma t$

$$-\frac{1}{\rho}\frac{\partial p}{\partial y}=\frac{\mathrm{d}U_y}{\mathrm{d}t}+P_y \tag{7}$$

where $U_y=u_b\cos\phi\cos\sigma t$. P_x and P_y=constants.
Finally, the components of the shear stress τ_{zx} and τ_{zy} in Eqs. (1) and (2) are related to the velocity gradients $\partial U/\partial z$ and $\partial V/\partial z$ as follows:

$$\tau_{zx}=\rho\nu_T\frac{\partial U}{\partial z},\quad \tau_{zy}=\rho\nu_T\frac{\partial V}{\partial z} \tag{8}$$

The distribution of turbulent energy $k(z,t)$ is determined by solving a transport equation for this quantity. The scheme involves a relationship between turbulent energy $k(z,t)$, eddy viscosity $\nu_T(z,t)$, mixing length $l(z,t)$, and dissipation rate ϵ. The eddy viscosity is dependent upon the distribution of turbulent energy, which is governed by the equation

$$\frac{\partial k}{\partial t}=\nu_T\left[\left(\frac{\partial U}{\partial z}\right)^2+\left(\frac{\partial V}{\partial z}\right)^2\right]+\alpha\frac{\partial}{\partial z}\left(\nu_T\frac{\partial k}{\partial z}\right)-\epsilon \tag{9}$$

where α=ratio of the eddy diffusivities of energy and momentum. The terms on the right-hand side of Eq. (9) represent energy generation, diffusion, and dissipation rates, respectively. The dissipation occurs mainly in the very small eddies and is given by the turbulence scaling law

$$\epsilon=C_2k^{3/2}/l \tag{10}$$

The bottom boundary condition on Eq. (9) is of zero energy flux

$$\nu_T\frac{\partial k}{\partial z}=0 \tag{11}$$

Three types of boundary conditions were implemented for use at the free surface:

1. Dirichlet boundary condition for stress-driven boundary layers, which was first used for a wind forced surface by Mellor and Yamada (1982) and obtained from the assumption that production and dissipation of turbulent energy are equivalent near the free surface

$$k=2C_2^{-2/3}U_f^2 \tag{12}$$

where C_2=empirical constant and U_f=friction velocity.

2. The no-flux condition proposed for use even on a shear-driven boundary by Burchard et al. (1998)

$$\nu_T\frac{\partial k}{\partial z}=0 \tag{13}$$

After Burchard et al. (1998) we found negligible differences, except in the very upper layer, between no-flux Eq. (13) and Dirichlet Eq. (12) boundary conditions for the mean velocity profile. However, in a pressure gradient-driven channel flow without wind forcing, only condition (13) guarantees that the eddy viscosity converges to a small value near the surface (see Burchard et al. 1998). This approach can be generalized to include wave breaking (see Craig and Banner 1994), where the injection of turbulent kinetic energy through the sea surface is modeled by the nonhomogeneous Neumann condition (3).

3. A Neumann boundary condition arises when considering the influence of surface gravity waves on the transport of turbulent energy. Craig and Banner (1994) specify the input of turbulent kinetic energy, which is assumed to result from breaking waves of all scales. The influence of breaking waves may be incorporated into the model as a source of energy at the surface. The energy input is assumed, on dimensional grounds, to be proportional to the cube of the friction velocity induced by both local wind and radiation stresses

$$\alpha C_1 l\sqrt{k}\frac{\partial k}{\partial z}=\psi U_f^3 \tag{14}$$

where ψ=empirical constant; l=mixing length; and parameter C_1=dimensionless constant.

The choice of the boundary condition in the present model is optional and depends on flow conditions (different driving forces, breaking waves, and nonbreaking waves) to which the model is applied. As the energy k is contained mainly in the large-scale fluctuations, $k^{1/2}$ is a velocity scale for the eddies with most of the kinetic energy. A measure for the size of these eddies is the length scale l. When these scales are used in the eddy viscosity relation, then

$$\nu_T=C_1lk^{1/2} \tag{15}$$

This formula is known as the Kolmogorov–Prandtl expression.

The following form of mixing length proposed by Davies (1990) was used in the current work (for details see Perlin 2000):

$$l=\kappa k^{1/2}D\left[\int_{z_0}^{z}k^{-1/2}dz+z_0k_0^{-1/2}\right] \tag{16}$$

where the damping function D was found to be (in accordance with experiments of Nezu and Rodi 1986)

$$D=\sqrt{(1-z/h)} \tag{17}$$

Celik and Rodi (1984) suggested the use of a ''surface damping function'' to reduce the mixing length from a mid-depth maximum to zero at a free surface. In order to satisfy the condition that the length scale cannot vanish at the upper boundary, its value can be set equal to κz_{01}, where z_{01}=the surface roughness length (Burchard et al. 1998). Thereby, Eq. (16) was changed into the form

$$l=\kappa\left\{k^{1/2}D\left[\int_{z_0}^{z}k^{-1/2}dz+z_0k_0^{-1/2}\right]+z_{01}\frac{z}{h}\right\} \tag{18}$$

To estimate surface roughness, Craig (1996) compared the measurements of wave velocities in the near-surface profile of Cheung and Street's (1988) experiments with results of calculations by a turbulence closure model. The experiments were conducted in a wind tunnel with wind blowing over water approximately 1 m deep. In their numerical turbulence model the mixing length l varies linearly away from each of the top and bottom boundaries as

$$\begin{aligned} l&=\kappa(z_{01}+h-z), & (h-z_{01}+z_0)/2\leqslant z\leqslant h\\ l&=\kappa(z_{01}+z), & 0\leqslant z\leqslant(h-z_{01}+z_0)/2 \end{aligned} \tag{19}$$

with Neumann [Eq. (13)] surface boundary conditions for the turbulent energy. For all experiments it was found that surface roughness z_{01} varies between 2 and 20 mm. According to sensitivity analysis it was shown that the overall solution, except for a small variation in the upper part of the flow, is not sensitive to the changes in surface roughness even over wider limits. The average surface roughness z_{01} was chosen to be equal to 10 mm. This final form of the mixing length distribution Eq. (19) was used in the current work.

The system of equations was rendered dimensionless and a

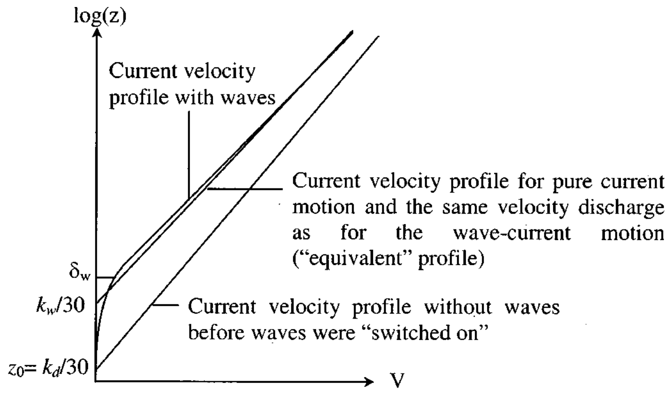

Fig. 1. Mean velocity profile with and without waves

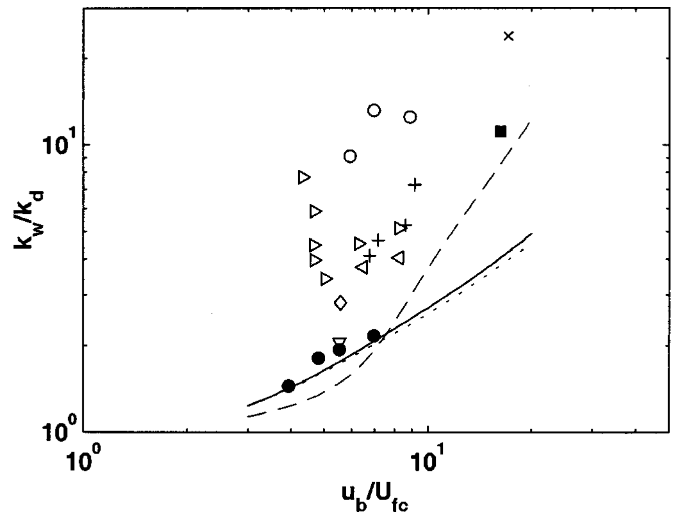

Fig. 2. Apparent roughness as function of U_b/u_{fc}. $A/k_d=0.8$ (dotted line), $A/k_d=1.2$ (solid line), $A/k_d=33$ (dashed line), (●) Kemp and Simons (1982); following current; (+) Kemp and Simons (1983); opposing current; (◇) Asano and Iwasaki (1984); opposing current, case III; (▽) Asano et al. (1986); case IV, opposing current; (■) Klopman (1994); following current; (×) Klopman (1994), opposing current; (▷) Mathisen and Madsen (1996a,b); (◁) Mathisen and Madsen (1996a,b); following current; (○) Fredsøe et al. (1999); following current. For experiments details see Table 6 in Fredsøe et al. (1999).

log–linear depth transformation was applied to provide more computational levels in the bottom boundary layer, with a linear distribution of computational levels near the free surface (for details see Perlin 2000). The Crank–Nicholson finite difference method was used to solve the transformed equations and corresponding boundary conditions.

The validation of the model requires comparison of the velocity profiles and turbulence properties with field and experimental data and with those produced by other models. Davies (1986) compared results of his model with the theoretical results of Kajiura (1968) and the empirical results of Jonsson (1967); Kamphuis (1975), and Jonsson and Carlsen (1976). Several authors have made comparisons between Davies (1986) model results and the latter data, e.g., Justesen (1988) using the "$k-\epsilon$" model. Justesen also compared his results with the data of Sumer et al. (1987) and Sleath (1987). Comparisons have also been made between model prediction and experimental results for combined wave–current flow by Simons et al. (1988) for mean velocity and turbulent intensity measured with a laser Doppler anemometer. Further comparisons have been made between the predictions of the model and observations of the vertical structure of a tidal current at a site in the Celtic Sea (see King et al. 1985).

In summary, a range of comparisons with data for waves alone, current alone, and combined wave–current flow, and also with the predictions of other models, has led to the conclusion that the model provides generally convincing predictions for *both* mean velocity and turbulence energy. The model was tested against laboratory measurements performed by Jensen et al. (1989) who investigated turbulent oscillatory boundary layers at high Reynolds numbers. It should be stressed that the data of Jensen et al. (1989) allows testing *time-dependent distributions* of velocity, turbulence energy, and shear stress. It was concluded from this comparison that the model provides suitable means for time-dependent vertical distributions of velocity, turbulence energy, and shear stress in the wave boundary layer (Perlin 2000).

The method of obtaining wave roughness from the model implemented in the present work is as follows. When waves are "switched on" on the steady current, mean current velocity is retarded due to increased bottom resistance (see Fig. 1). When convergence of the wave–current motion is achieved, waves are removed from the motion and substituted by pure current motion. In order to keep the same (reduced) water discharge as for the wave–current motion, bed roughness is replaced by a larger value (since driving forces are held constant at their initial values). The bed roughness is replaced by the larger values gradually until the required mean current velocity is achieved. As a result, the "apparent" roughness, that provides the same mean velocity for the current alone configuration as in the case of wave–current motion, is obtained. This method for the determination of k_w, involving constancy of water discharge, differs from the definition used by most other workers. The usual convention is that adopted by Fredsoe et al. (1999), i.e., k_w is determined directly from the mean wave–current velocity profile. As may be seen from Fig. 1 of the present paper, this difference in definition will lead to a consistent underestimate of k_w compared to the classical definition.

The model described above implicitly assumes homogeneously distributed roughness. Nevertheless, it is interesting to test out its applicability for a rippled bottom. The experimental results of different authors presented by Fredsøe et al. (1999), as given in Fig. 13 of their paper, are compared to runs of our model (Fig. 2). As discussed above, the curves computed using the model should be raised to some extent, but it does not essentially change the agreement with the experimental results. For example, the k_w/k_d values represented by the dashed line should be increased by about 15–20% to correspond to the classical definition of apparent roughness, but this difference would be hardly seen since the vertical axis (k_w/k_d) is in logarithmic scale. The parameters for the computations have been chosen in accordance with the data presented in Table 6 of Fredsøe et al. (1999). The results show that the model performs better for bottoms with evenly distributed roughness (Klopman's experiment), rather than bottoms covered by two-dimensional artificial ripples or bars (all other experiments). This limits the model's applicability to exclude the lab results of Mathisen and Madsen (1996a,b), and Fredsøe et al. (1999), who studied the importance of organized bed roughness generating coherent vortices. It is most likely that the turbulence in the boundary layer will be affected significantly by these vortices. The model cannot distinguish between following and opposing waves, but performs better for following waves.

Climate and Bathymetry Conditions

The analysis of the climate and bathymetry conditions is necessary to set up the computational domain for simulations. The results presented here relate to practical applications for the Israeli coast but can be employed on other sandy beaches when the main subject of interest is focused on longshore sediment transport. The coastal region of Israel is characterized by small tidal waves and, correspondingly, weak tidal currents. Prevailing currents in the near-shore area are the wave-driven longshore currents. Outside of the breaking zone the energy dissipation is weak and shear radiation stress, which drives the longshore current, is almost constant. Inside the breaking zone, the energy dissipation is strong, and the shear component of the radiation stresses decrease toward the shoreline. The imbalance in the shear radiation stress must be compensated through the bed shear stress associated with the longshore current. As a first approximation, the shear radiation stress can be assumed to act on the free surface (see Fredsøe and Deigaard 1992). Breaking waves can drive strong currents in the surf zone. At the same time, high turbulence associated with the waves brings a large amount of sediment into suspension. That suspended sediment is transported along the coast by a longshore current. Finally, the longshore current determines the morphological development in the coastal region. The vertical structure of the flow depends on the four dimensionless groups (k_d/h), (U_c/u_b), (A/k_d), and (ϕ), formed by six parameters, namely: bed roughness k_d, water depth h, mean current velocity for the current alone U_c, amplitude of the wave orbital velocity u_b, amplitude of the wave orbital motion A, and mutual orientation of waves and current ϕ. In order to find the upper and lower limits of these dimensionless groups and select the most representative values, estimations of sediment drift in the Israel coastal area and possible wave–current situations are performed. The estimations are based on wave data measured simultaneously in Ashdod and Haifa as well as bathymetry data measured along the Israeli coast (Perlin and Kit 1999a). Wave transformation and the longshore currents, generated by waves, are simulated utilizing the *LITPACK* package, *LITPACK user's guide and reference manual* (1998), Danish Hydraulics Institute. Though *LITPACK* does not allow for the simulation of 3D flow patterns, it enables rough cross-sectional estimates of flow and sediment transport. The main characteristics of the wave–current climate, sediment and bathymetry data, and sediment drift on the Israeli coast, following from these estimations, are given below.

Typical Israeli seabed profiles are described in detail by Kit and Pelinovsky (1998). Mean grain size diameter d_{50} and grain size distribution d_{84}/d_{16} on the Tel Aviv coast (Perlin and Kit 1999b) are about $d_{50}\sim 0.17$ mm and $d_{84}/d_{16}\sim 1.3$. The active region, where significant sediment drift occurs, is located through 0.5–8 m depth in accordance with the gross transport (see Fig. 3). The net transport, which is usually considered as the most important since it is responsible for beach erosion or accumulation, can be misleading in this sense (i.e., the determination of the active region) due to the balance between northerly and southerly drifts. The bottom profile on Fig. 3 originates from Ashkelon (Kit and Pelinovsky 1998). The ripples are washed out in the region where the sediment transport is significant (breaking zone). In most simulations, the bed roughness is accounted for in the same manner as for a fixed bed and taken as $k_d = 2.5 d_{50}$. However, a number of simulations are also performed for higher bed roughness to account for the effect of mobile sand beds (Nielsen 1992), and here a representative bed roughness has been chosen as $k_d = 80 d_{50}$.

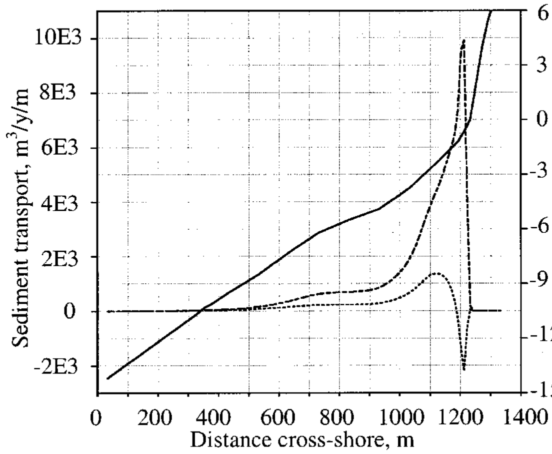

Fig. 3. Distribution of sediment transport along off-shore profile: (solid line) bottom track; (dashed line) gross transport, and (dotted line) net transport

Table 1 demonstrates the contribution of waves with various heights to sediment transport. The estimations are based on calculations for 4-year time series wave data in the Ashdod area by applying the modified Coastal Engineering Research Center formula (Perlin and Kit 1999a). It is clearly seen that waves lower than 1 m can be neglected because of their small contribution to sediment transport. Therefore, only waves higher than 1 m are taken into account. Maximum deep water RMS wave height H_{RMS} is about 3.5 m. Peak wave periods T_{peak}, that correspond to the above mentioned minimum and maximum wave heights, are approximately 6 and 13 s, respectively. To select a number of typical situations, a statistical analysis of wave data has been performed. Nine representative waves that define sediment transport in the Tel Aviv area, which are similar to sediment transport calculated from the wave time series, have been selected.

The analysis of the transformation of these representative waves is performed utilizing the *LITDRIFT* module of the *LITPACK* package and the following results are obtained. Near-bed wave orbital velocity varies through 0.5–1.4 m/s. Amplitude of near-bed wave orbital motion varies in the range 0.5–2.5 m. Mean wave generated longshore current varies through 0–1.5 m/s, though in the breaking zone, mean current is 0.2 m/s and higher. Far from marine structures the wave driven currents are in the longshore direction. Though the angle ϕ between waves and current varies from 0° to 90°, it is worth emphasizing that in most

Table 1. Estimations of Contributions of Waves with Different Wave Height to Sediment Transport

RMS deep water wave height (cm)	Contribution (%)
0–50	2.7
50–100	2.9
100–150	15
150–200	14.5
200–250	17.7
250–300	22.5
>300	24.7

situations when wave height exceeds 1 m, waves are superimposed on the currents at an angle between 70° and 90°, because currents are in the longshore direction far from marine structures and high waves are always coming from directions close to normal to the shoreline. The statistics of wave directions is discussed in detail in Kit and Perlin (1999).

Therefore, the following ranges of flow and seabed properties are of interest for the current study:

$$0.5\ \text{m}<h<10\ \text{m}$$

$k_d \sim 0.5$ mm (fixed bed roughness), 14 mm (movable bed roughness)

$$\left.\begin{array}{r} 1\ \text{m}<H_{\text{RMS}}<3.5\ \text{m} \\ 6\ \text{s}<T_{\text{peak}}<13\ \text{s} \end{array}\right\} \quad \begin{array}{c} 0.5\ \text{m/s}<u_b<1.5\ \text{m/s} \\ 0.5\ \text{m}<A<2.5\ \text{m} \end{array}$$

$$0.1\ \text{m/s}<U_c<1.5\ \text{m/s}$$

$$0°<\phi<90°$$

The limits of dimensionless groups have been found by introducing extreme values of the dimensional parameters into the dimensionless expressions. The most representative values (selected in bold) have been chosen according to the distribution of the most probable combinations of the dimensional parameters

$$k_d/h = 0.5E-4, \mathbf{1E-4}, \mathbf{2E-4}, 1E-3\ (k_d = 2.5 d_{50});$$

$$1E-3, 3E-3, 3E-2\ (k_d = 80 d_{50})$$

$$A/k_d = 1{,}000, \mathbf{3{,}000}, 6{,}000\ (k_d = 2.5 d_{50}),$$

$$33, 100, 200\ (k_d = 80 d_{50})$$

$$U_c/u_b = 0.1, 0.2, \mathbf{0.5}, \mathbf{0.7}, \mathbf{1}, 2$$

$$\phi = 0°, 45°, \mathbf{70°}, \mathbf{80°}, \mathbf{90°}$$

Not all combinations of these situations are possible in practical cases. For example, parameters A and u_b are dependent on one another and low values of k_d/h are possible only in relatively "deep" water, beyond the breaking zone, where only low values of the group $U_c/u_b = 0.1$, 0.2 are expected.

It is important to obtain the apparent bed roughness for at least a "rough" matrix of a possible combination of these dimensionless groups. In the present work, a limited number of combinations of dimensionless groups are studied. Nevertheless, the studied cases enable us to find a functional dependence of the apparent roughness on the dimensionless groups.

Apparent Bed Roughness Evaluation

Dependence of Wave Roughness on Flow Properties

The results presented below show the dependence of the wave roughness on wave, current, and morphological properties. The model has been run for values of the nondimensional groups described above, but dependencies are plotted mostly for the nondimensional group $U_{fc}/u_b = \sqrt{\tau_b/\rho}/u_b$ instead of U_c/u_b because U_{fc} is considered to be prescribed (τ_b for the stationary motion should be equal to the vector sum of the driving forces). U_{fc} in this expression is the mean friction velocity; τ_b is the bed shear stress and ρ is the fluid density. Therefore, U_{fc} is the known variable, while U_c is obtained during solution. Figs. 4(a and b) show the curves of normalized apparent bed roughness (k_w/k_d) plotted against relative bed roughness (k_d/h). Curves are plotted for the most representative angle (80°) between waves and current. In Fig. 4(a) these curves are plotted for $A/k_d = 6{,}000$ (fixed bed roughness, i.e., sandpaper, $k_d = 2.5 d_{50}$) and in Fig. 4(b) for $A/k_d = 100$ (bed roughness, which accounts for the effect of mobile sand bed, $k_d = 80 d_{50}$). In the wide range of U_{fc}/u_b and for both values of A/k_d, the dependence of normalized apparent bed roughness on relative bed roughness is negligible. Indeed, if we assume that turbulence is generated mostly by waves, and that thickness of the turbulent wave boundary layer is small relative to the depth, then the wave boundary layer should not be affected by the entire depth and changes in water depth should not influence the wave boundary layer.

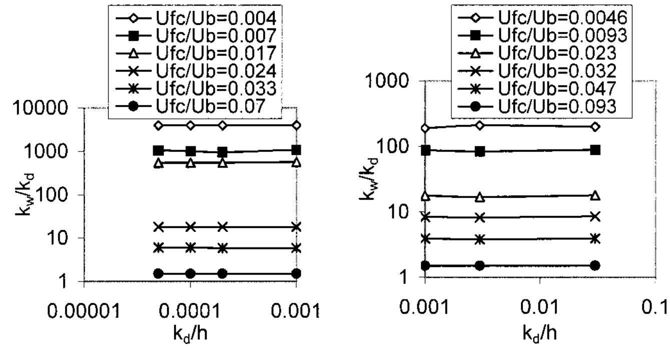

Fig. 4. Dependence of apparent roughness on relative bed roughness: (left plot) $A/k_d = 6{,}000$, (right plot) $A/k_d = 100$

Figs. 5 and 6 demonstrate the dimensionless apparent roughness (k_w/k_d)-[Figs. 5(a) and 6(a)] and time-averaged depth-mean wave–current velocity scaled by velocity of the current in isolation (U_{cw}/U_c)-[Figs. 5(b) and 6(b)], plotted against mutual orientation of the current and wave motions. The computations are made for $k_d/h = 1E-4$ (fixed bed roughness) and $A/k_d = 1{,}000$, 3,000, and 6,000 (Fig. 5), and for $k_d/h = 3E-3$ (movable bed roughness) and $A/k_d = 100$ (Fig. 6). Six different values of U_c/u_b have been chosen: 0.1, 0.2, 0.5, 0.7, 1, and 2 (U_{fc}/u_b correspondingly 0.0033, 0.0068, 0.0165, 0.0231, 0.034, and 0.068 for fixed bed roughness and 0.0046, 0.0093, 0.0231, 0.0324, 0.0465, and 0.0931 for movable bed roughness). It follows from the Figs. 5 and 6 that the dependence of the apparent roughness on the mutual orientation of current and wave motion in the range between 70° and 90° is weak. That range covers most of the practical cases, at least when sediment transport is significant (i.e., for waves higher than 1 m). Situations, when mutual orientation of waves and current is less than 70°, occur only in the areas around marine structures. In those cases the influence of mutual orientation grows with a decrease in the angle between waves and current and a maximum influence can be seen for the collinear case. Between 70° and 0° the change in $\log(k_w/k_d)$ is close to linear, the inclination of the lines depending on parameters U_{fc}/u_b and A/k_d. For high values of A/k_d (fixed bed roughness), the dependence of the apparent bed roughness on the angle is higher for the cases when the wave orbital velocity and current velocity are almost equal. For small waves on a strong current, or high waves on weak current, dependence on their mutual orientation decreases. For low values of A/k_d, the stronger the current relative to the wave orbital velocity, the higher the dependence on ϕ. The fact that Figs. 5(a) [6(a)] and 5(b) [6(b)] look similar when the parameter k_w/k_d is plotted on a logarithmic scale and U_{cw}/U_c on a linear scale reflects the tendency toward the logarithmic velocity distribution in boundary layer flow.

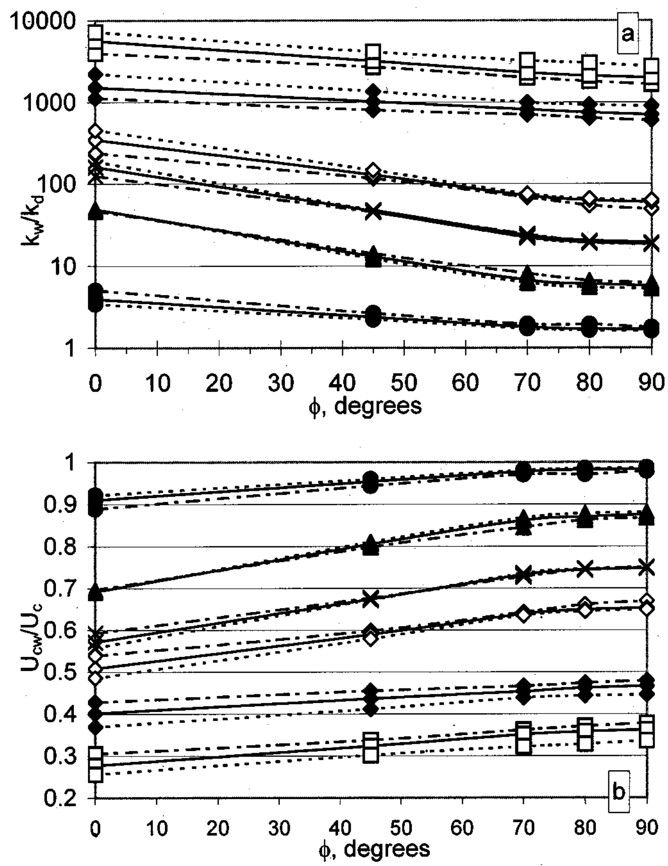

Fig. 5. Dependence of normalized apparent bed roughness (a) and current reduction (b) on mutual orientation of waves and current. Fixed bed roughness: (dot-dashed line) $A/k_d = 1E3$, (solid line) $A/k_d = 3E3$, (dashed line) $A/k_d = 6E3$, (□) $U_c/u_b = 0.1$, (♦) $U_c/u_b = 0.2$, (◇) $U_c/u_b = 0.5$, (×) $U_c/u_b = 0.7$, (▲) $U_c/u_b = 1$, and (●) $U_c/u_b = 2$.

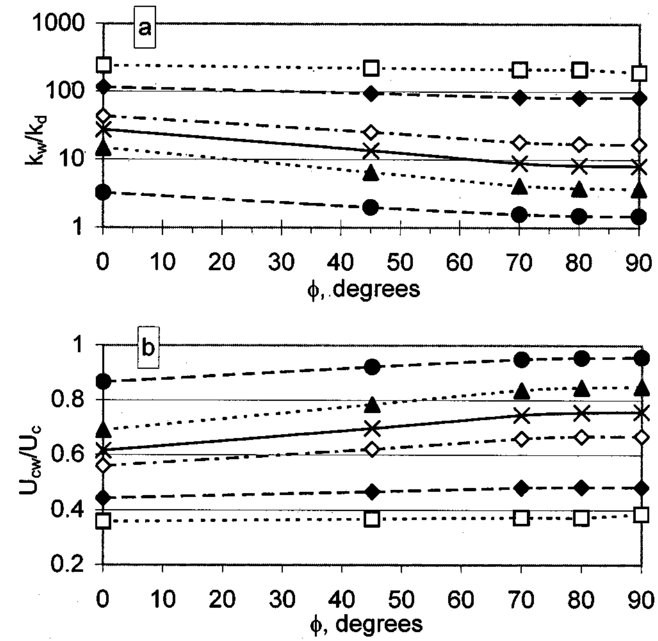

Fig. 6. Dependence of normalized apparent bed roughness (a) and current reduction (b) on mutual orientation of waves and current. Movable bed roughness $A/k_d = 100$: (□) $U_c/u_b = 0.1$, (♦) $U_c/u_b = 0.2$, (◇) $U_c/u_b = 0.5$, (×) $U_c/u_b = 0.7$, (▲) $U_c/u_b = 1$, and (●) $U_c/u_b = 2$.

In Fig. 7 the variations in dimensionless apparent roughness as a function of U_c/u_b [Fig. 7(a)] and U_{fc}/u_b [Fig. 7(b)] are shown for different values of A/k_d ($A/k_d = 6{,}000$, 1,000, 200, 100, and 33). The variations are shown for an 80° angle between waves and current. The dependence of the apparent bed roughness on the group U_c/u_b (U_{fc}/u_b) is very strong and normalized apparent bed roughness increases as the group U_c/u_b (U_{fc}/u_b) decreases. In fact, the groups U_c/u_b and U_{fc}/u_b characterize the relation between wave and current turbulent intensities. It is interesting to note that the curves on Fig. 7(b) cross each other, which means that the apparent roughness for a relatively weak current (i.e., small values of U_{fc}/u_b, less than 0.025) is smaller for small values of A/k_d. This means that for fixed u_b and k_d, apparent roughness is larger for the fast oscillations in the case of relatively strong currents. The opposite applies for the case of a relatively weak current.

Approximate Expression for Functional Dependence of Apparent Bed Roughness on Flow Properties

As shown above, the nondimensional apparent bed roughness k_w/k_d depends mostly on three groups: U_{fc}/u_b, A/k_d, and ϕ. Dependence on group k_d/h is very weak and can be neglected. Fig. 7(b) demonstrates the dependence of $\log(k_w/k_d)$ on the nondimensional groups U_{fc}/u_b and A/k_d. Approximation of this de-

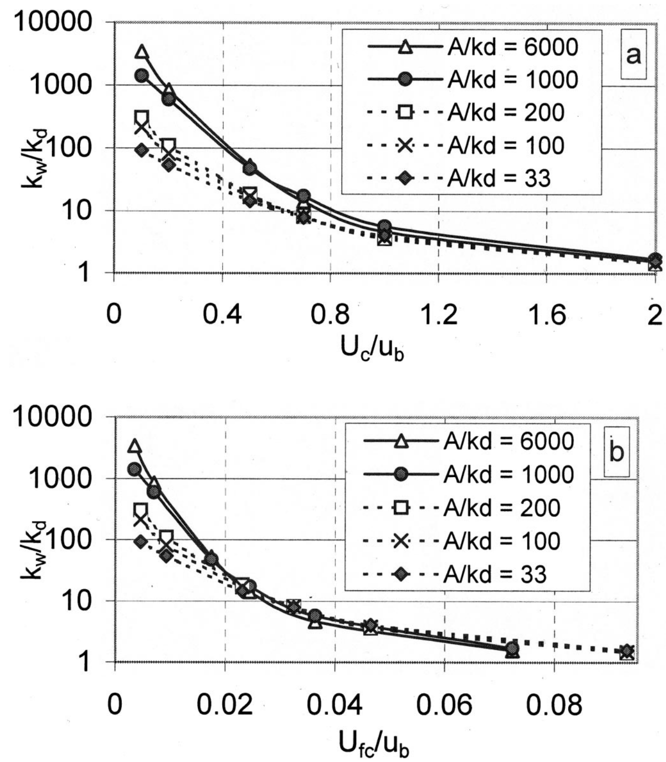

Fig. 7. Dependence of normalized apparent bed roughness on group U_c/u_b (a) and U_{fc}/u_b (b): (△) $A/k_d = 6{,}000$, (●) $A/k_d = 1{,}000$, (□) $A/k_d = 200$, (×) $A/k_d = 100$, and (♦) $A/k_d = 33$

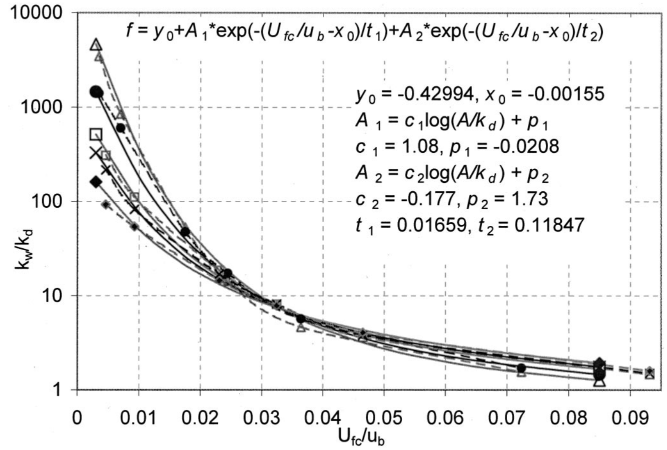

Fig. 8. Fitting of dependence of apparent bed roughness on groups U_{fc}/u_b and A/k_d: (dashed lines) model runs, (solid lines) fitting expression, (△) $A/k_d=6{,}000$, (●) $A/k_d=1{,}000$, (□) $A/k_d=200$, (×) $A/k_d=100$, and (♦) $A/k_d=33$

pendence enables one to readily conduct the evaluation of the apparent bed roughness when the mutual orientation of waves and current is close to normal and other input parameters are allowed to vary. The fitting function [Eq. (20)], which approximates this dependence, represents the sum of two exponents dependent upon group U_{fc}/u_b, the coefficients of these exponents being logarithmic functions of group A/k_d

$$\log(k_w/k_d)=f(U_{fc}/u_b, A/k_d)$$
$$=y_0+A_1\exp(-(U_{fc}/u_b-x_0)/t_1)$$
$$+A_2\exp(-(U_{fc}/u_b-x_0)/t_2) \qquad (20)$$

where f=fitting function; t_1, t_2, y_0, and x_0=coefficients: $t_1=0.0166$, $t_2=0.1185$, $y_0=-0.43$, and $x_0=-0.00155$; A_1, A_2=functions of the group A/k_d: $A_1=c_1\log(A/k_d)+p_1$ and $A_2=c_2\log(A/k_d)+p_2$, where $c_1=1.08$, $p_1=-0.0208$, $c_2=-0.177$, and $p_2=1.73$. For fixed bed roughness, the approximate expression could be simplified. The dependence on group A/k_d can be neglected and coefficients A_1 and A_2 could be substituted by constants: $A_1=3.72$ and $A_2=1.08$. Graphs for the fitting function are plotted in Fig. 8.

The dependence of the apparent bed roughness on the mutual orientation of the waves and currents in the most relevant situations (when the angle between waves and current is between 90° and 70°) is insignificant. Nevertheless, between 70° and 0° that dependence should be accounted for. The dependence of $\log(k_w/k_d)$ on ϕ has also been approximated for the fixed bed roughness. Linear approximation fits well and the inclination angle of the linear dependence is defined by parameters A/k_d and U_{fc}/u_b, i.e.,

$$\log(k_w/k_d)=f \quad \text{for } 70°\leqslant\phi\leqslant 90°$$
$$\log(k_w/k_d)=f+G_f(1.22-\phi) \quad \text{for } 0°<\phi<70° \qquad (21)$$

where G_f=slope coefficient and ϕ=expressed in radians.

The approximating expression G_f is obtained by the best fit of the discrete values of G found as described above (see Fig. 9)

$$G_f=y_{10}+2\sum_{i=1,2}B_iw_i/\pi/(w_i^2+4(U_{fc}/U_b-x_{ci})^2) \qquad (22)$$

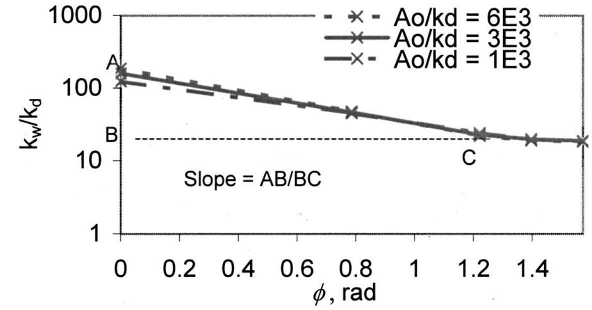

Fig. 9. Example of linear fitting function for apparent roughness dependence on angle between wave and current directions: ac is fitting line; G is slope; $U_c/u_b=0.7$

where $y_{10}=0.023$; $B_1=0.0497$; $B_2=0.00773$; $w_1=0.0492$; $w_2=0.0186$; $x_{c1}=0.0385$; and $x_{c2}=0.022$. The dependence of G on U_{fc}/u_b and its approximation for fixed bed roughness G_f is demonstrated in Fig. 10.

There should be one more constraint on the wave roughness calculated utilizing the approximating expression (20). The wave roughness should be limited in relation to the water depth. The entire water depth h is chosen as a criterion for the upper limit of wave roughness and the bed roughness k_d is chosen as the lower limit. The hyperbolic tangent is used in order to provide continuity at the upper limit. Thus, the final form of the approximating function is as follows:

$$\frac{k_w}{k_d}=\frac{h}{k_d}\tanh\left(\frac{k_d}{h}10^f\right) \quad \text{for } 70°\leqslant\phi\leqslant 90°$$
$$\frac{k_w}{k_d}=\frac{h}{k_d}\tanh\left(\frac{k_d}{h}10^{f+G_j(1.22-\phi)}\right) \quad \text{for } 0°<\phi<70° \qquad (23)$$

Therefore, for the fixed bed roughness, Eq. (23) allows calculations of k_w/k_d for any input parameters of waves and current. For the arbitrary bed roughness (at least in near-shore conditions where ripples are mostly washed out), this formula results in similar accuracy of the apparent roughness as the numerical turbulence closure model does for the mutual orientation of waves and current between 90° and 70° that covers most possible cases. The result obtained from the approximate equation is within a few percent from the one calculated by implementing the numerical model.

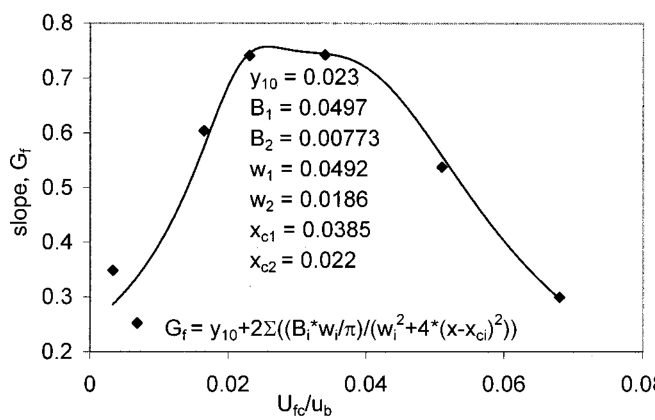

Fig. 10. Best fit of slope coefficient G_f: (diamonds) slope coefficient; (solid line) fit

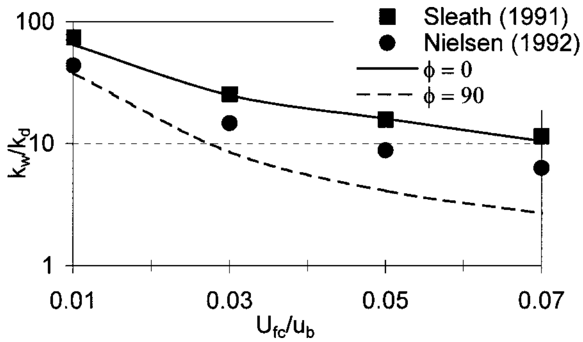

Fig. 11. Apparent roughness computations for $A/k_d=15$ by different approximate expressions derived by Sleath (1991); Nielsen (1992); and in current research

A comparison of the computations of the apparent bed roughness by the approximate expression (23) with the results obtained applying other approximations is shown below. Sleath (1991) developed a model, which leads to the expression

$$\frac{k_w}{k_d}=1+0.19\frac{u_b}{U_{fc}}\sqrt{\frac{A}{k_d}} \tag{24}$$

and Nielsen (1992) derived an expression for a constant, real-valued eddy viscosity in the wave boundary layer.

$$\frac{k_w}{k_d}=0.44\frac{u_b}{U_{fc}} \tag{25}$$

The expressions obtained by Sleath (1991) and Nielsen (1992) are valid only for small values of A/k_d, i.e., for fairly large relative roughness. Sleath's (1991) expression is valid in the range $1<A/k_d<120$ and the expression derived by Nielsen (1992), which does not include dependence on A/k_d, is valid only for $2<A/k_d<17$. Both these expressions do not include dependence on mutual orientation of waves and current.

A comparison among the three relations is performed for fixed value $A/k_d=15$. For such a large value of relative bed roughness, the approximating expression obtained in the present research allows computation of the apparent roughness only for mutual orientation of waves and current between 70° and 90°. The estimations of apparent roughness for waves and current propagating in the coinciding direction ($\phi=0°$) have been obtained based on numerical simulations (Fig. 6). It can be clearly seen from Fig. 11 that in all cases the apparent roughness, obtained from Nielsen's (1992) expression, lies between values computed for $\phi=90°$ and $\phi=0°$, and apparent roughness obtained from Sleath's (1991) expression almost coincides with that for $\phi=0°$. The indubitable advantage of the expression derived in the present research is that it allows computations in a very wide range of A/k_d and accounts for mutual orientation of waves and current. The applicability of A/k_d values as low as 15 have been verified using this expression versus the full model and a very reasonable agreement between computed values of apparent roughness was obtained.

Implementation of Apparent Bed Roughness in Three-Dimensional CAMERI Model

The 3D CAMERI flow model (Sladkevich et al. 2000) was used to calculate the flow pattern in the Tel Aviv region for a number of wave situations. The flowchart in Fig. 12 demonstrates how the apparent bed roughness, calculated using the approximate expres-

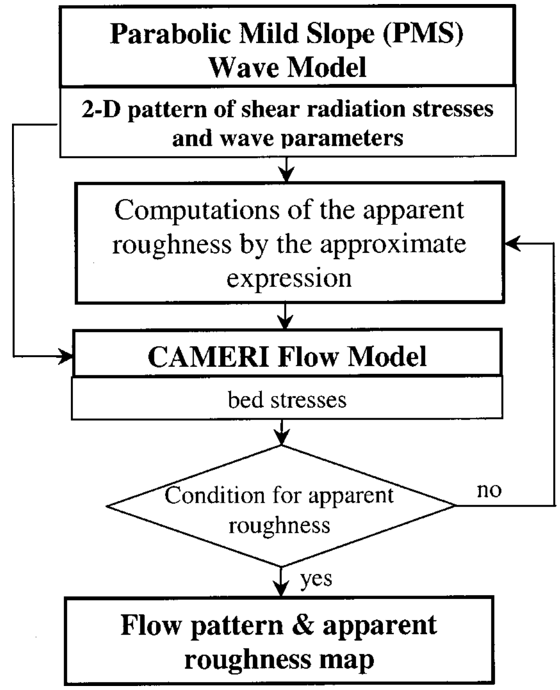

Fig. 12. Flowchart for implementation of apparent bed roughness to three-dimensional CAMERI flow model

sion (23), was implemented for calculating flow patterns by the 3D CAMERI flow model. Wave transformation on the coast was calculated using the parabolic mild slope (PMS) module of the *MIKE21* package, *MIKE21 user's guide and reference manual* (1995), Danish Hydraulic Institute. The approach of Battjes and Janssen (1978) has been used to model irregular waves. The model has been applied with a 5×5 m grid. The 2D maps of wave characteristics (RMS wave height and direction) and radiation stresses were obtained as output from the PMS module.

The wave parameters computed using the PMS module serve as input for the approximate expression (23). Wave roughness, from expression (23), is calculated for the cases when turbulent ($\mathsf{R}>6E5, \mathsf{R}=A^2\sigma/\nu$) (Nielsen 1992) or transitional ($3E5<\mathsf{R}<6E5$) regimes are observed in the bottom boundary layer. In these expressions R is the Reynolds number, σ is the wave frequency, and ν is the kinematic viscosity. For the transitional regime the logarithm of ratio k_w/k_d has been decreased proportionally with the Reynolds number. For the laminar regime, bed roughness is left unchanged. To evaluate the flow pattern using the CAMERI model, the wave roughness map is used as an input parameter for the CAMERI flow model along with the radiation stress field. Grid size in a CAMERI flow model changes from 15 m in the breaking zone near the structures to 200 m at the boundaries far from the analyzed region. Time step depends on a stability criterion and approximately varies around 1 min. A no-flux condition has been applied on the sea structures and on the solid boundaries. The feedback from the CAMERI model for roughness calculations is realized by using bed stresses from the CAMERI model to calculate a second approximation of the wave roughness map. The bed stresses are not equal to shear radiation stresses, even in steady flow, since the latter account for the additional stresses caused by horizontal nonuniformity of the flow. Then, the second approximation of the flow pattern is calculated. The iterations stop when the integral $\int_x\int_y \log(k_w/k_d)$ over the simulated domain, computed in successive iterations, converges

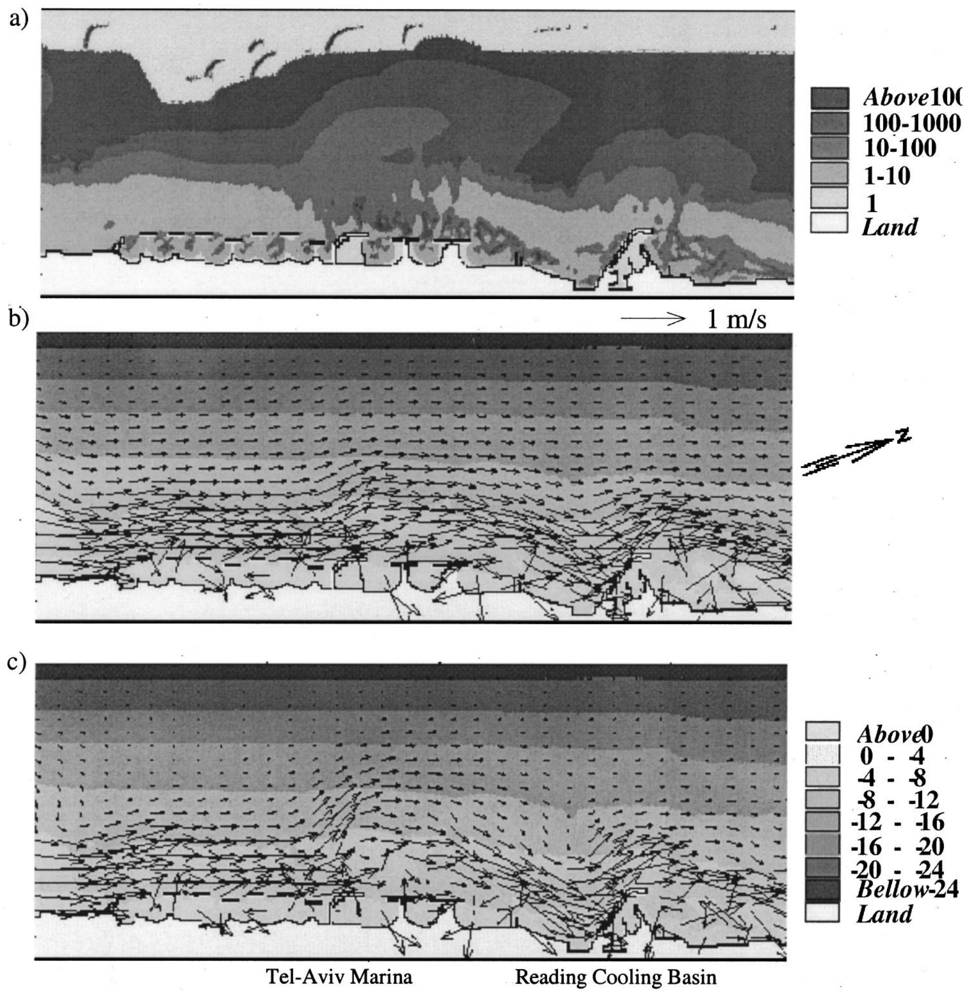

Fig. 13. Flow simulations for wave No. 1 ($H=275$ cm, $T=11.2$ s, $\theta_0=278°$). Tel-Aviv coast: (a) ''apparent'' roughness maps, (b) flow pattern calculated without implementation of ''apparent'' roughness map, and (c) flow pattern calculated with implementation of ''apparent'' roughness map.

to within 10% between these iterations. In all modeled cases three iterations were enough for convergence.

In the present research, two typical storm (out of nine) conditions corresponding to waves arriving from south and north directions have been chosen for simulations. The relative roughness maps for these conditions are shown in Figs. 13(a) and 14(a). In these figures θ_0 is the direction of the wave vector, relative to the north, and the direction of the normal to the shoreline at the chosen location (Tel Aviv coast) $\theta_s=284°$. Wave roughness differs significantly from bed roughness, e.g., the ratio k_w/k_d reaches 1,000 and even more in the outer zone beyond the breaking. In this region ripples can be present and it is unclear if the apparent roughness computed using a plane sandy bed would give accurate results. However, it is obvious that the roughness in this region is essentially magnified due to wave action and the trend is correct. In the surf zone, where the radiation stresses are induced and a longshore current is generated, the ratio k_w/k_d rarely exceeds 100. Two couples of flow patterns (for flow with and without implementation of the apparent bed roughness) for two wave conditions are shown in Figs. 13(b and c) and 14(b and c) for waves 1 and 2, respectively. The results indicate that the flow calculated without wave roughness implementation differs significantly from that calculated with wave roughness implementation. The difference can be seen both in the magnitude of current velocities and in the direction of current propagation. Flow velocities calculated with the implementation of wave roughness have significantly smaller magnitudes. For example, the magnitude of mean current velocity on the seaside of marine structures for wave condition No. 1, without implementation of the apparent roughness [Fig. 13(a)], varies between 0.35 and 1.0 m/s, with a mean velocity of about 0.85 m/s. With implementation of the apparent roughness [Fig. 13(b)] the magnitude varies between 0.25 and 0.7 m/s, with mean velocity 0.65 m/s. For wave condition No. 2, the magnitude of flow velocity on the seaside of marine structures in Fig. 14(a) (without wave roughness) varies between 0.3 and 0.95 m/s, with mean velocity 0.65–0.7 m/s, and in Fig. 14(b) (with wave roughness) the magnitude varies between 0.2 and 0.7 m/s, with mean velocity of about 0.5 m/s.

Deflection of flow velocities in the cross-shore directions near marine structures for flow calculated with implementation of wave roughness, compared to the flow calculated without implementation of wave roughness, is also clearly seen (Figs. 13 and 14). For example, for wave condition No. 1 (Fig. 13), the flow is shifted in the offshore direction near the Tel Aviv Marina and in front of the cooling basin of the Reading power station. For wave condition No. 2 (Fig. 14) at a depth of 8 m and more to the south of Reading, there are circulation cells for computations with wave roughness, while in computations without wave roughness the

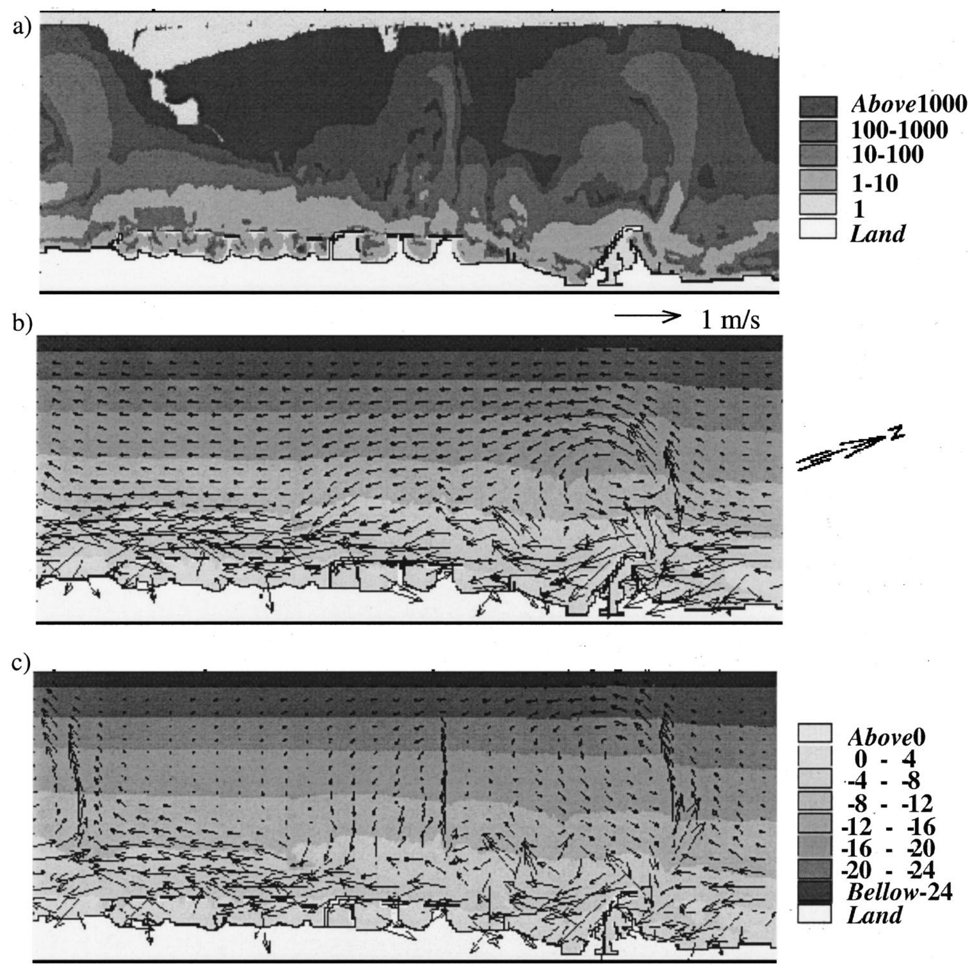

Fig. 14. Flow simulations for wave No. 2 ($H=240$ cm, $T=10.5$ s, $\theta_0=297°$). Tel Aviv coast: (a) ''apparent'' roughness maps, (b) flow pattern calculated without implementation of ''apparent'' roughness map, and (c) flow pattern calculated with implementation of apparent roughness map

flow is just parallel to the shoreline. In front of Reading, a circulation cell in Fig. 14(b) is shifted to deeper water. From the sediment transport point of view, deflection of the current in the presence of marine structures, when taking into account wave roughness in the CAMERI flow model, should automatically increase cross-shore sediment transport and, respectively, bypassing of marine structures by sediments.

Concluding Remarks

In the present research a numerical turbulence closure model of the type used by Davies et al. (1988) and Davies (1990) was developed. The described model differs from the Davies (1990) model by introducing a shear stress on the free surface as a boundary condition instead of zero velocity gradient, and by the possibility of using different boundary conditions for turbulent equation on the free surface. A sensitivity analysis reveals that the overall solution is not sensitive to changes in surface roughness. The model is implemented for computations of the apparent bed roughness.

Typical wave–current situations for the Israeli near-shore conditions are studied, and limiting and also most typical values of the wave and current characteristics are selected. Wave–current motion in the near-shore conditions is defined by four dimensionless groups, namely k_d/h, U_{fc}/u_b (U_c/u_b), A/k_d, and ϕ. Dependence of wave roughness on all dimensionless groups is studied. It is shown that changes in the parameter k_d/h do not have much effect on the solution. The dependence of the apparent roughness on the groups U_{fc}/u_b, A/k_d and mutual orientation of waves and current ϕ is important and could be nonmonotonous in different ranges of parameters. It is shown that in most practical situations, which are significant for sediment transport, the mutual orientation of waves and current varies between 70° and 90°. The dimensionless group U_{fc}/u_b is the most important and actually defines the apparent roughness variation.

A fitting technique for results obtained by solving the numerical turbulence closure model has been used to derive an empirical expression that associates the apparent roughness with dimensionless groups U_{fc}/u_b, A/k_d, and ϕ. The use of this approximating expression eliminates the necessity for performing heavy numerical simulations. Maps of the apparent roughness for the Tel Aviv coast have been obtained for particular wave conditions utilizing the approximate expression. These maps were implemented in the 3D CAMERI flow model.

The flow computations, accounting for the increase of apparent bed roughness caused by the turbulence induced by the waves, lead to a flow pattern that differs significantly from that obtained by the neglect of wave generated turbulence. The implementation of the apparent bed roughness in the 3D model enables evaluation of physically more reasonable flow patterns.

A comparison of flow patterns calculated with and without apparent roughness shows that accounting for apparent roughness in flow calculation results in the decrease of current velocities and divergence of the velocity field around marine structures. It should be emphasized that the approach suggested in the current work is of a general nature and is not limited for the Israeli coast only.

Acknowledgments

This work has been supported by an INTAS Grant. The assistance of CAMERI researchers, Dr. M. Sladkevich and Dr. M. Gluzman is highly appreciated.

Notation

The following symbols are used in this paper:

A = near bed wave excursion amplitude;
A_1, A_2 = empirical constants;
B_1, B_2 = empirical constants;
C_1, C_2 = empirical constants;
c_1, c_2 = empirical constants;
D = damping function;
d_{16}, d_{50}, d_{84} = grain size exceeding by weight 16, 50, and 84% of particles, respectively;
f = fitting function;
G = slope coefficient;
G_f = approximation of slope coefficient;
H = wave height;
H_{RMS} = RMS wave height;
H_0 = deep water wave height;
h = water depth;
k = turbulent kinetic energy;
k_d = bed roughness;
k_w = apparent bed (wave) roughness;
k_0 = turbulent energy at z_0;
l = mixing length;
P_x, P_y = constants;
p = mean pressure;
p_1, p_2 = empirical constants;
R = Reynolds number;
T = wave period;
T_{peak} = peak wave period;
t = time;
t_1, t_2 = empirical constant;
U = horizontal component of velocity in x direction;
U_c = mean current velocity for current alone;
U_f = friction velocity;
U_{fc} = friction velocity of mean current;
u_b = amplitude of near-bed wave orbital velocity;
V = horizontal component of velocity in y direction;
V_0 = free stream velocity;
w_1, w_2 = empirical constants;
x = horizontal coordinate in direction normal to shoreline;
x_{c1}, x_{c2} = empirical constants;
x_0 = empirical constant;
y = horizontal coordinate in direction parallel to shoreline;
y_0 = empirical constant;
z = vertical coordinate;
z_0 = level of zero velocity;
z_{01} = surface roughness length;
α = ratio of eddy diffusivities of energy and momentum;
δ_c = current bottom boundary layer thickness;
δ_{cw} = wave–current bottom boundary layer thickness;
ϵ = dissipation rate;
κ = von Kármán constant;
ν = kinematic molecular viscosity;
ν_T = eddy viscosity;
ρ = density of fluid;
σ = wave frequency $2\pi/T$;
τ_b = bed shear stress;
τ_s = surface shear stress;
τ_{zx}, τ_{zy} = Reynolds stress in x direction/y direction, respectively;
ϕ = angle between wave and current; and
ψ = empirical constant.

References

Arnskov, M. M., Fredsøe, J., and Sumer, B. M. (1993). "Bed shear stress measurements over a smooth bed in three-dimensional wave-current motion." *Coastal Eng.*, 20, 277–316.

Asano, T., and Iwagaki, Y. (1984). "Bottom turbulent boundary layer in wave-current coexisting systems." *Proc., 19th Int. Conf. on Coastal Engineering*, Houston, 2397–2413.

Asano, T., Nakagawa, M., and Iwagaki, Y. (1986). "Changes in current properties due to wave superimposing." *Proc., 20th Int. Conf. on Coastal Engineering*, Taipei, Taiwan, 925–939.

Battjes, J. A., and Janssen, J. P. F. M. (1978). "Energy loss and set-up due to breaking of random waves." *Proc., 16th Int. Conf. Coastal Engineering*, ASCE, New York, 509–587.

Bobyleva, L. M., Zilitinkevich, S. S., and Laikhtman, D. L. (1965). "Turbulent regime in a thermally stratified planetary atmospheric boundary layer." *Proc., Int. Colloquium on the Microstructure of the Atmosphere and the Effect of Turbulence on Radiowave Propagation*, Moscow.

Burchard, H., Petersen, O., and Rippeth, T. P. (1998). "Comparing the performance of the Mellor-Yamada and the $k-\epsilon$ two equation turbulence models." *J. Geophys. Res., [Oceans]*, 103(C5), 10543–10554.

Celik, I., and Rodi, W. (1984). "Simulation of free-surface effects in turbulent channel flows." *PCH, PhysicoChem. Hydrodyn.*, 5(3/4), 217–227.

Cheung, T. K., and Street, R. L. (1988). "The turbulent layer in water at an air–water interface." *J. Fluid Mech.*, 194, 133–151.

Christoffersen, J. E., and Jonsson, I. G. (1985). "Bed friction and dissipation in a combined current and wave motion." *Ocean Eng.*, 12, 387–423.

Coffey, F. C., and Nielsen, P. (1985). "Aspects of wave current boundary layer flows." *Proc., 19th Int. Conf. on Coastal Engineering, 1984*, ASCE, New York, 2232–2245.

Coffey, F. C., and Nielsen, P. (1986). "The influence of waves on current profiles." *Proc., 20th Int. Conf. on Coastal Engineering, 1984*, ASCE, Taipei, 82–96.

Craig, P. D. (1996). "Velocity profiles and surface roughness under breaking waves." *J. Geophys. Res., [Oceans]*, 101(C1), 1265–1277.

Craig, P. D., and Banner, M. L. (1994). "Modeling wave-enhanced turbulence in the ocean surface layer." *J. Phys. Oceanogr.*, 24, 2546–2559.

Davies, A. G. (1986). "A numerical model of the wave boundary layer." *Cont. Shelf Res.*, 6, 715–739.

Davies, A. G. (1990). "A model of the vertical structure of the wave and current bottom boundary layer." *Modeling marine systems*, A. M.

Davies, ed., Vol. 2, Chap. 10, CRC, Boca Raton, Fla, 263–297.
Davies, A. G. (1991). "Transient effects in wave-current boundary layer flow." *Ocean Eng.*, 18, 75–100.
Davies, A. G., Soulsby, R. L., and King, H. L. (1988). "A model of the vertical structure of the wave and current bottom boundary layer." *J. Geophys. Res., [Oceans]*, 93(C4), 491–508.
Fredsøe, J. (1984). "Turbulent boundary layer in wave-current motion." *J. Hydraul. Eng.*, 110(8), 1103–1120.
Fredsøe, J., Andersen, K. H., and Sumer, B. M. (1999). "Wave plus current over ripple-covered bed." *Coastal Eng.*, 38, 177–221.
Fredsøe, J., and Deigaard, R. (1992). *Mechanics of coastal sediment transport*, World Scientific, Singapore.
Grant, W. D., and Madsen, O. S. (1979). "Combined wave and current interaction with a rough bottom." *J. Geophys. Res., C: Oceans Atmos.*, 84(C4), 1797–1808.
Jensen, B. L., Sumer, B. M., and Fredsøe, J. (1989). "Turbulent oscillatory boundary layers at high Reynolds numbers." *J. Fluid Mech.*, 206, 265–297.
Jonsson, I. G. (1967). "Wave boundary layers and friction factors." *Proc., 10th Int. Conf. Coastal Engineering*, ASCE, New York, 127.
Jonsson, I. G., and Carlsen, N. A. (1976). "Experimental and theoretical investigations in an oscillatory turbulent boundary layer." *J. Hydraul. Res.*, 14, 45.
Justesen, P. (1988). "Prediction of turbulent oscillatory flow over a rough bed." *Coastal Eng.*, 12, 257–284.
Kajiura, K. (1968). "A model of the bottom boundary layer in water waves." *Bull. Earthquake Res. Inst., Univ. Tokyo*, 46, 75.
Kamphuis, J. W. (1975). "Friction factor under oscillatory waves." *J. Waterw., Harbors, Coastal Eng. Div., Am. Soc. Civ. Eng.*, 101(2), 135–144.
Kemp, P. H., and Simons, R. R. (1982). "The interaction between waves and a turbulent current: waves propagating with the current." *J. Fluid Mech.*, 116, 227–250.
Kemp, P. H., and Simons, R. R. (1983). "The interaction between waves and a turbulent current: waves propagating against the current." *J. Fluid Mech.*, 130, 73–89.
King, H. L., Davies, A. G., and Soulsby, R. L. (1985). "A numerical model of the turbulent boundary layer beneath surface waves and tides." *Rep. No. 196*, Inst. of Oceanographic Science, Taunton, England.
Kit, E., and Pelinovsky, E. (1998). "Dynamical models for cross-shore transport and equilibrium bottom profiles." *J. Waterw., Port, Coastal, Ocean Eng.*, 124(3), 138–146.
Kit, E., and Perlin, A. (1999). "Longshore sediment drift on the coast of Israel." *Proc., 5th Int. Conf. on Coastal and Port Engineering (COPEDEC V)*, G. P. Mocke, ed., Cape Town, South Africa, 68–79.
Klopman, G. (1994). "Vertical structure of the flow due to waves and current." *Progress Rep. No. H840.30, Part II, Delft Hydraulics, prepared for Rijkwaterstaat, Tidal WaterDivision and Commission of the European Communities*, Directorate General XII , Delft, The Netherlands.
Li, Z., and Davies, A. G. (1996). "Towards predicting sediment transport in combined wave-current flow." *J. Waterw., Port, Coastal, Ocean Eng.*, 122(4), 157–164.
Lodahl, C. R., Sumer, B. M., and Fredsøe, J. (1998). "Turbulent combined oscillatory flow and current in a pipe." *J. Fluid Mech.*, 373, 313–348.
Lundgren, H. (1973). "Turbulent currents in the presence of waves." *Proc., 13th Int. Conf. on Coastal Engineering, 1972*, ASCE, New York, 623–634.
Madsen, O. S. (1991). "Simple models for turbulent wave-current bottom boundary layer flow." *Dredging Research Program; Final Rep.*, Washington, D.C.
Mathisen, P. P., and Madsen, O. S. (1996a). "Waves and current over a fixed ripped bed: Bottom roughness experienced by waves in the presence and absence of currents." *J. Geophys. Res., [Oceans]*, 101(C7), 16533–16542.
Mathisen, P. P., and Madsen, O. S. (1996b). "Waves and current over a fixed ripped bed: Bottom roughness experienced by currents in the presence of waves." *J. Geophys. Res., [Oceans]*, 101(C7), 16543–16550.
Mellor, G. L., and Yamada, T. (1982). "Development of a turbulence closure model for geophysical fluid problems." *Rev. Geophys.*, 20, 851–875.
Myrhaug, D. (1984). "A theoretical model of combined wave and current boundary layers near a rough bottom." *Proc., 3rd Int. Symp. on Offshore Mechanics and Arctic Engineering*, J. S. Chung, ed., ASME, New York, 559–568.
Nezu, I., and Rodi, W. (1986). "Open-channel flow measurements with a laser Doppler anemometer." *J. Hydraul. Eng.*, 112(5), 335–355.
Nielsen, P. (1992). *Coastal bottom boundary layers and sediment transport*, World Scientific, Singapore.
Nikuradse, J. (1932). *Gesetzmässigkeiten der turbulenten Ströming in glatten Rohren*, VDA-Forschungsheft, Berlin.
Perlin, A. (2000). "Development of some aspects of a global sedimentological transport model at the Israeli coast." PhD thesis, Tel Aviv Univ., Tel Aviv, Israel.
Perlin, A., and Kit, E. (1999a). "Longshore sediment transport on Mediterranean coast of Israel." *J. Waterw., Port, Coastal, Ocean Eng.*, 125(2), 80–87.
Perlin, A., and Kit, E. (1999b). "Wave climate evaluation for sedimentological studies." *Proc., Int. MEDCOAST Conf. on Wind and Wave Climate of the Mediterranean and the Black Sea (NATO TU-WAVES Project)*, Antalya, Turkey, 237–250.
Simons, R. R., Grass, A. J., and Mansour-Tehrani, M. (1992) "Bottom shear stresses in the boundary layer under waves and currents crossing at right angles." *Proc., 23rd Int Conf. on Coastal Engineering*, Venice, Italy, 604–617.
Simons, R. R., Kyriacou, A., Soulsby, R. L., and Davies, A. G. (1988). "Predicting the nearbed turbulent flow in waves and currents." *Proc., IAHR Symp. on Mathematical Modeling of Sediment Transport in the Coastal Zone*, Copenhagen, Denmark.
Sladkevich, M., Militeev, A. N., Rubin, H., and Kit, E. (2000). "Simulation of transport phenomena in a shallow aquatic environment." *J. Hydraul. Eng.*, 126(2), 128–136.
Sleath, J. F. A. (1987). "Turbulent oscillatory flow over rough beds." *J. Fluid Mech.*, 182, 369.
Sleath, J. F. A. (1990). "Velocities and bed friction in combined flows." *Proc., 22nd Int. Conf. on Coastal Engineering*, ASCE, Delft, The Netherlands, 450–463.
Sleath, J. F. A. (1991). "Velocity and shear stresses in wave-current flows." *J. Geophys. Res., [Oceans]*, 96(C8), 15237–14244.
Smith, J. D. (1977). "Modeling of sediment transport on continental shelves." *The sea*, E. D. Goldberg et al., eds., Vol. 6, Interscience, New York, 539–577.
Sumer, B. M., Jensen, B. L., and Fredsøe, J. (1987). "Turbulence in oscillatory boundary layers." *Advances in turbulence*, G. Comte-Bellot and J. Mathieu, eds. Springer, Berlin, 556.
Tanaka, H., Chian, C. S., and Shuto, N. (1983). "Experiments on an oscillatory flow accompanied with a unidirectional motion." *Coast. Eng. Japan*, 26, 19–37.
Tanaka, H., and Shuto, N. (1981). "Friction coefficient for a wave current coexisting system." *Coast. Eng. Japan*, 24, 105–128.
von Kármán, Th. (1930). "Mechanische ähnlichkeit und turbulenz." *Nach. Ges. Wiss. Göttingen, Math. Phys. Klasse*, 58.